Engineering Structures 131 (2017) 1–13

Contents lists available at ScienceDirect

Engineering Structures

journal homepage: www.elsevier.com/locate/engstruct

A nonlinear model for multilayered rubber isolators based on a co-rotational formulation

N. Maureira [a,b,*], J. de la Llera Ph.D [b], C. Oyarzo Ph.D [a], S. Miranda [b,c]

[a] Faculty of Engineering, Universidad Católica de la Santísima Concepción, Chile
[b] National Center for the Integrated Management of Natural Disasters (CIGIDEN), CONICYT/FONDAP/15110017, Faculty of Engineering, Pontificia Universidad Católica de Chile, Chile
[c] School of Engineering, Universidad del Desarrollo, Chile

ARTICLE INFO

Article history:
Received 17 August 2015
Revised 3 May 2016
Accepted 26 September 2016
Available online 2 November 2016

Keywords:
Multilayer rubber isolator
Non-linear behavior
Axial-lateral coupling
Tension and compression buckling
Time-history analysis

ABSTRACT

This article proposes a geometrically nonlinear co-rotational model aimed to characterize the mechanical behavior of elastomeric seismic isolators. The model is able to capture the axial and lateral coupling in both axial directions, i.e. compression and tension of the isolator. Also reproduces the instability the loads in tension as well as in compression, and provides theoretical evidence of the non-symmetric behavior of the isolator in these two directions. To validate model results, a quasistatic analysis was performed on a typical isolator with many different shape factors. From the parametric analysis performed, it is observed that buckling loads are higher in tension than in compression. However, as the shape factor of the isolator increases, the behavior in compression and tension becomes symmetric. It becomes apparent that significant differences in normal stresses and strains under tensile and compressives loads are observed for axial loads smaller than 10% of the nominal buckling load. The example presented shows that lateral displacements of about ±25% of isolator radius and tension forces up to 10% of the buckling load are possible without inducing cavitation in the rubber. Accuracy of the model was also tested against finite element model results and experimental data showing satisfactory results. Furthermore, a response-history analysis of an isolated structure is presented and compared for two isolator models: the two-spring model and the model proposed herein. Finally, material nonlinearity was introduced in the dynamic analysis using a Bouc-Wen type element in parallel with the isolator. The responses are similar between models; however, significant differences occur locally in the isolator for high axial loads and/or large lateral displacements.

1. Introduction

Until recent years, the use of seismic isolation was constrained to squat and heavy structures [1,2]. This is due to the fact that taller structures have longer periods, and the isolation response reduction due to period lengthening decreases as the period of the structure increases. Moreover, taller buildings may undergo large overturning moments that induce high axial loads on the isolators, with high risk of uplift of the building and of crushing of the devices, which may result in excessive tensile or compressive stresses on them. However, experience shows that a good number of taller buildings still experience a significant benefit if seismic isolation is used, not only in terms of reducing their base shear, but also in controlling their interstory deformations due to lateral and torsional motions of the superstructure [3]. Therefore, for these cases it is necessary to understand and model in detail the axial behavior of isolators in order to design them correctly.

The axial behavior of rubber isolators has been studied in the past by theoretical and experimental means [4–6]. It has been experimentally demonstrated that elastomeric isolators perform very well under high compressive stresses [4,5], as opposed to their behavior under high tensile stresses [6], which may cause cavitation in the rubber. This behavior is independent of eventual bonding failures between rubber and steel shims, since for well manufactured isolators the rupture always occurs in the elastomeric material, and not at the rubber-steel interface [7].

In buildings, the axial behavior of isolators under earthquake loads implies a superposition of other stresses caused by shear and bending. Theoretical and experimental results have demonstrated that isolators subjected to axial load and lateral displacement present a significant reduction in their equivalent lateral stiffness due to second order geometric effects, and in critical

* Corresponding author at: Faculty of Engineering, Universidad Católica de la Santísima Concepción, Alonso de Ribera 2850, Concepción, Chile.
E-mail addresses: nmaureira@ucsc.cl (N. Maureira), jcllera@ing.puc.cl (J. de la Llera), coyarzov@ucsc.cl (C. Oyarzo), smirand@uc.cl (S. Miranda).

http://dx.doi.org/10.1016/j.engstruct.2016.09.055
0141-0296/

Nomenclature

Notation

MSM denotes the model presented herein, called "Multi-springs model"

TSM denotes the model developed by Koh and Kelly [10], called "Two-springs model"

FEM denotes the finite element model developed in the software COMSOL to validate the results of the MSM

R, N, t_r, t_s radius of the isolator, number of rubber layers, rubber layer thickness and steel shim thickness, respectively

S, A, H_r, H first shape factor, cross section area of the isolator, total height of rubber, and total height of the isolator

G, K shear modulus and Bulk modulus of the rubber

E_c, EI_{eff} compression modulus, and effective flexural modulus of the rubber layer

X_n, Y_n, Z_n local co-rotated axes of the n-th rubber layer; origin is in the centroid of area of the deformed layer

X, Y, Z global axes of the isolator; origin is in the centroid of area of the lower face of the bottom rubber layer

$\Delta\alpha_n$, α_n, $\tilde{\alpha}_n$ relative rotation between opposite faces of n-th rubber layer, absolute rotation of the local axis X_n and absolute rotation of the n-th steel shim, respectively

M_n, M_y bending moment at the mid-plane of the n-th rubber layer, and on top of the isolator, respectively

M_y^H, M_y^0 bending moments on upper face (positive clockwise) and lower face (positive anti-clockwise) of isolator

$p_t = [V_x, P_z]^T$ vector of global load acting on upper face of the isolator; include global shear and axial loads

$p_n = [V_n, P_n]^T$ vector of local load acting on the mid-plane of the n-th rubber layer; include local shear and axial loads

$\boldsymbol{v_g^n} = [u_x^n, w_z^n]^T$ relative displacements in global axes, between lower face of the n-th rubber layer and steel shim above

$\boldsymbol{v_n} = [u_n, w_n]^T$ vector of relative displacement in local axes, between opposites faces of the n-th rubber layer

$\boldsymbol{v_t} = [u_x, w_z]^T$ vector of displacement on top end of the isolator in global axes

$\boldsymbol{v_g^{(n)}} = [u^{(n)}, w^{(n)}]^T$ vector of absolute displacement in global axes, of the centroid of volume of the n-th rubber layer

$\boldsymbol{R_n}, \boldsymbol{r_n}, \boldsymbol{s_n}$ kinematic matrix and vectors dependent on loads. They come from the co-rotational formulation

$\boldsymbol{F}, \overline{\boldsymbol{F}}$ flexibility matrix of a single rubber layer and flexibility matrix dependent on loads of the complete isolator

$\boldsymbol{r_g^{(n)}}$ coordinates of the centroids of the n-th rubber layer in undeformed configuration, in global axes

$\boldsymbol{r_g^{(n)}} = [x_o^{(n)}, z_o^{(n)}]^T$ coordinates of the origin of local axes of the n-th rubber layer, projected on global axes

$\boldsymbol{s_g^{(n)}} = [x^{(n)}, z^{(n)}]^T$ vector of global displaced coordinates of a generic point of the border of the n-th rubber layer

$\boldsymbol{v_n}(x_n, z_n)$ vector of local displacement of a generic point of the border of the n-th rubber layer. $\boldsymbol{v_n} = [u_{Xn}, w_{Zn}]^T$

$\gamma_n, \gamma_{x_n z_n}, \gamma_{y_n z_n}$ shear strain due to local shear load V_n, and total shear strain within rubber in local axes due to V_n, P_n, M_n

$\tau_{x_n z_n}, \tau_{y_n z_n}$ total shear strain within rubber in local axes, due to shear load, axial load and bending moment

$\sigma_{x_n}, \sigma_{y_n}, \sigma_{z_n}$ normal stress within the rubber due to local loads V_n, P_n, M_n

$\varepsilon_{x_n}, \varepsilon_{y_n}, \varepsilon_{z_n}$ normal strain within the rubber due to local loads V_n, P_n, M_n

conditions could even become unstable [8,9]. This coupled behavior between axial load and lateral displacement is responsible for the geometrically non-linear behavior of a multilayer rubber bearing isolator. Because in typical buildings the diaphragm system above the isolation interface is usually very stiff in bending, this study assumes no rotation of the isolator at the interface with the diaphragm and substructure.

Several mathematical models have been proposed earlier in the literature to predict the axial behavior of isolators. Koh and Kelly [10] were the first in proposing a simple mechanical model to characterize the nonlinear geometric behavior of the isolator that incorporates axial-lateral coupling. Later, Chang [11] used Haringx's theory—which considers the slope of the deformed longitudinal axis and the rotation of the section of a rubber column as independent variables—in developing a non-linear model for the coupled mechanical behavior of an elastomeric isolator through an analytical 4×4 stiffness matrix. With a different approach, Kelly [12] developed a model based on a homogenization of the complete isolator column as a continuum element using also Haringx's theory and imposing to originally plane sections to remain plane, but not perpendicular to the deformed longitudinal axis of the element. This analysis shows theoretically that an isolator may buckle in compression and tension with identical buckling loads. However, in practice, buckling in tension is anticipated by cavitation of the rubber [12]. More recently, Ryan et al. [5], proposed an extension of the two-spring model proposed earlier [10] by introducing the inelastic behavior of a lead-core in lead-rubber isolators. This last model is capable of representing the geometrically non-linear global behavior of the isolator, the elastic behavior of the rubber, and the inelastic hysteretic behavior of the yielding lead core. Variations of these models have also been proposed elsewhere [4], which propose to characterize the nonlinear geometric behavior of the isolator by a bed of axial springs at the top and bottom edges and an axial and shear spring to represent the isolator. The hysteretic behavior is added by a global force-deformation constitutive relationship of the device, and hence, the model may represent the behavior of a lead core and/or to include inelasticity in the rubber.

Furthermore, Liu et al. [13] studied the behavior of isolators in states of pure compression and compression plus shear. Based on the vertical stiffness and deformation theory, a series of concepts were introduced and related with the theory to develop a representative model of the overall mechanical behavior of the isolator. As an extension to this work, this group of researchers incorporated in the isolator model tension and tension plus shear [13,14]. They also included a bilinear model of rubber. More recently, He et al. [15] using Haringx's model and an inelastic rotational stiffness developed a simplified mechanical model to represent isolators in bending, compression, and shear, including the effect of a lead core.

All these previous models are based on the behavior of the isolator as a complete unit, and with the sole exception of [11], do not build the global behavior of the isolator from the local behavior of the individually deformed layers of steel and rubber. Consequently, the proposed model characterizes first the axial and lateral behavior of each steel-rubber layer in local coordinates, and derives from it, the overall coupled behavior of the isolator by transforming this local axes behavior into global axes.

The aim of this research was to propose a nonlinear mathematical model based on a co-rotational formulation capable of

representing the overall behavior of a multilayer elastomeric isolator considering axial-lateral coupling. The proposed model represents the global mechanical behavior and overall stability of the isolator, as well as the internal local response of the rubber in terms of stresses and strains. The model is capable of predicting cavitation, shear deformation capacity, and the overall instability conditions of the isolator due to a combination of shear and tension/compression loads. The article presents first the formulation of the constitutive behavior of the coupled axial-lateral isolator, resourcing mainly to a geometric approach. The analysis ensures the correct equilibrium equations for the internal rubber layers. The methodology is then used to solve this problem, and a series of results are interpreted to demonstrate the capabilities of the model and the types of results that can be obtained from it. A comparison of the response obtained using the proposed model with that of finite element models (FEM) and experimental results is also presented. A response-history analysis of an isolated structure is included to demonstrate the capacity of the proposed model in computing the dynamic response of a building. Finally, a comparison of the capacities of the proposed and existing models is included to better evaluate this proposal. Conclusions are finally drawn from these comparisons and the model characteristics.

2. Non-linear model approach

A key aspect to understand the coupling of lateral and axial behavior in an rubber isolator is to notice that as external lateral and axial loads are imposed onto the isolator, the kinematics of the deformation of horizontal internal rubber layers is such that they do not remain horizontal and rotate about the horizontal axis Y coming into the plane in Fig. 1(a). It turns out that the direction of this rotation caused by the lateral displacement in the X-direction is preserved if an external compression is added, but it may be inverted if an external tension force is applied. Indeed, this is the source of the asymmetric behavior of the isolator in tension and compression as seen later. This internal rotation of rubber layers causes that the external axial and shear forces have non-zero components on the local axes of each rubber layer (Fig. 1(b)).

Looking at Fig. 1, three important observations are made for the deformed configuration of the isolator. First, the component of the axial force parallel to the mid-plane of the rubber layer increases the magnitude of shear when there is compression, and hence generates an increase in lateral displacement, or a reduction in the equivalent lateral stiffness. Secondly, the vertical component of shear also adds to the compression force, thus causing a reduction in the equivalent vertical stiffness of the isolator. And thirdly, if there is tension—and its magnitude is not sufficiently large to change the direction of rotation of the rubber layers—the projection of this load on the mid-plane of each rubber layer is in opposite direction to the shear, thus generating an increase in lateral stiffness (tension stiffening). If tension is enough to change the sense of rotation of the layer, the applied shear deformation adds up to the one produced by tension, thus leading to a reduction in lateral stiffness. This is the reason for the asymmetric behavior in tension and compression.

2.1. Mathematical model

In this research a mathematical model is developed to characterize the geometric non-linear behavior of an elastomeric isolator using a corotational formulation. Most of this model is general and can be applied to a different geometry of isolators, by taking into account the corresponding changes in the load-displacement relationship of the single pad (Eqs. (1) and (2)). Due to the above, to maintain the generality of the proposed model, E_c and EI_{eff} in the equations are not specifically defined. However, these variables that depend on the cross section of the isolator, are well described in the literature [1].

The following hypotheses were considered for the model: (1) all rubber layers and steel shims are equal; (2) initially, rubber layers are considered as linear elastic elements; (3) Although axial-lateral coupling in layers is almost negligible, a couple of factors are defined in order to consider that effect; (4) all steel shims are assumed rigid elements and experience rigid body translation and rotation; and (5) the upper and lower end plates of the isolator remain horizontal due to the external building constraints. Consequently, peak rotation occurs at mid height and isolator deformations occur only in the rubber layers (Fig. 2).

The motivation for using a co-rotational model arises from the central observation that the rotation of rubber layers leads to the non-linear geometric behavior. A co-rotational formulation is specially appropriate to deal with this problem and develop a mathematical model that is simple enough to be reasonably accurate and computationally efficient. In a consistent co-rotational formulation, the following assumptions are considered: (1) nodal displacements can be large and include large rotations; (2) internal element deformations are considered small; (3) a fixed set of axes remains fixed to the studied element and solidarily rotates with it [16,17]. In the case of an elastomeric isolator these assumptions are met if the element considered is the constituent rubber layer. Therefore, translation of the origin of the co-rotated axes for each rubber layer is controlled by the large shear deformations of rubber

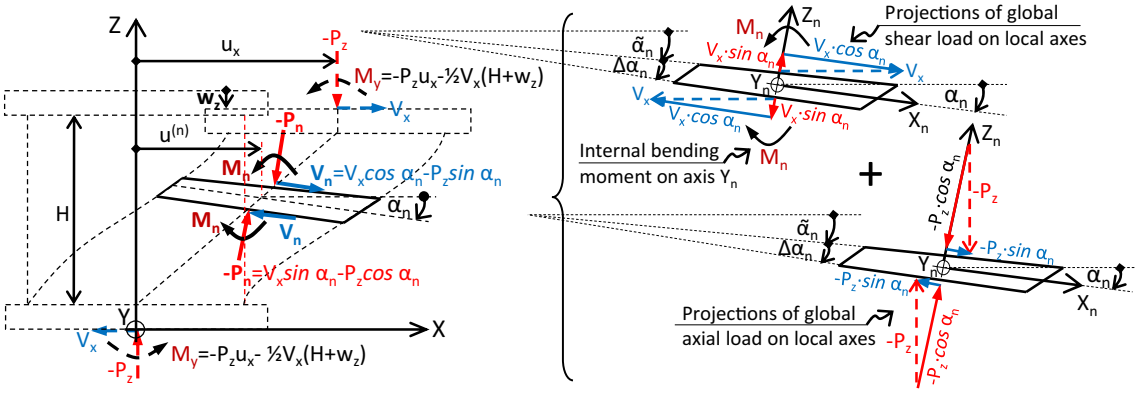

Fig. 1. Kinematics and equilibrium of an isolator: (a) external forces on the isolator (dashed arrows) and internal local forces on the n-th rubber layer (solid arrows); and (b) projection of the axial and shear forces on the local axes $X_n - Z_n$.

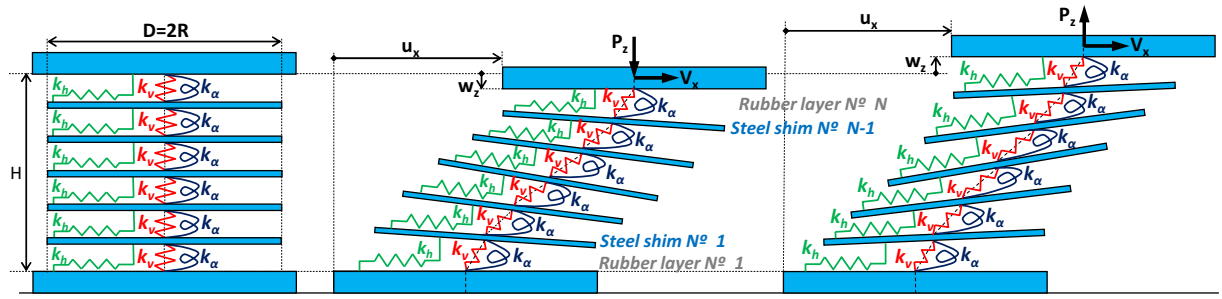

Fig. 2. Schematic representation of the multi-spring isolator model proposed (MSM): (a) undeformed configuration; (b) deformed configuration in shear and compression; and (c) deformed configuration in shear and tension.

layers. The stiffness matrices (or flexibility) of each constituent element are transformed according to this change between local and global coordinates.

Therefore, the development of the model requires the following: (1) to know the load-displacement relationship of the rubber layers in the local or co-rotated axes; (2) to define the rotation matrix of local axes; (3) to determine the translation of the origin of the local axes by considering large shear deformations; (4) to formulate the non-linear global load-displacement relationship; and (5) to develop a numerical algorithm that converges to the correct solutions starting from a given initial (guess) response.

2.2. Load-displacement relationship of a single rubber layer in local axes

Let us start by the well-known equilibrium of a single circular rubber layer [1] (Fig. 2). Local axes X_n, Y_n (into the plane), and Z_n are defined for the n-th rubber layer, whose origin is in the deformed position of the n-th rubber layer centroid (co-rotational formulation [16,17]). Considering that a typical elastomeric isolator is composed of many very thin rubber layers ($t_r \ll H$ or $N \gg 1$), the variation in bending moment across the rubber layer may be neglected. Therefore, in the model presented, the internal bending moment is considered constant across the layer and equals to the bending moment at the midplane of the layer, M_n. The above assumption implies that in determining the response of an elastic thin rubber layer, it can be assumed that the layer response for each internal force is uncoupled, which is a typical assumption of a co-rotational formulation [16,17]. Consequently, the model for a single rubber layer is identical to that presented elsewhere [18] as illustrated in Fig. 2.

The relationship between the local forces, displacements, and rotation of the n-th rubber layer (Fig. 2) is given by [1]

$$u_n = \frac{t_r}{GA} V_n; \quad w_n = \frac{t_r}{E_c A} P_n; \quad \Delta\alpha_n = \frac{t_r}{EI_{eff}} M_n \tag{1}$$

where the compression modulus E_c and the effective bending stiffness EI_{eff} can be obtained from the differential equations that rule the corresponding behavior of the rubber layer [1,2,19] considering the compressibility modulus of rubber, K. The solutions of the above equations depend on the geometry of the cross section of the isolator, and will not be written herein to maintain generality in the formulation.

The area A and the effective bending stiffness EI_{eff} in Eq. (1) are considered constant, even if the local shear displacement u_n is large. However, as the shear displacement increases, the area available to transfer the axial load (overlapping area) is reduced. Similarly, the inertia of that overlapping area is also reduced, which has an effect on the effective flexural stiffness. The above effect corresponds to a local axial-lateral coupling due to the large shear strains, and as a simple way to incorporate this effect into the model, the following reduction coefficients are defined for the area and stiffness: $f_A = \frac{\text{Overlaping SectionArea}}{\text{Cross SectionArea}} \leqslant 1$, and $f_I = \frac{\text{Overlaping SectionInertia}}{\text{Cross SectionInertia}} \leqslant 1$. The overlapping section area and inertia depend on the cross section of the isolator and the local shear displacement u_n. The expression is well-known and will not be repeated here [1,2]. These factors modify the last two expressions of Eq. (1) as follows:

$$w_n = \frac{t_r}{E_c A f_A} P_n; \quad \Delta\alpha_n = \frac{t_r}{EI_{eff} f_I} M_n \tag{2}$$

The fundamental assumption of the proposed model is that the vector of local displacements of the n-th rubber layer, $\boldsymbol{v_n} = [u_n, w_n]^T$, is a work conjugate pair of the vector of local forces, $\boldsymbol{p_n} = [V_n, P_n]^T$, and can be expressed in matrix form as follows:

$$\boldsymbol{v_n} = \begin{bmatrix} u_n \\ w_n \end{bmatrix} = \begin{bmatrix} t_r/(GA) & 0 \\ 0 & t_r/(E_c A f_A) \end{bmatrix} \cdot \begin{bmatrix} V_n \\ P_n \end{bmatrix} = \boldsymbol{F p_n} \tag{3}$$

where $\boldsymbol{F}$ is the rubber layer flexibility matrix.

2.3. Kinematic rotation matrix in local axes

The rigid-body rotation α_n of the n-th rubber layer relates the vector of displacements $\boldsymbol{v_g^n} = [u_x^n, w_z^n]^T$ (Fig. 4(b)) in global axes (X, Z) with the corresponding vector of displacements $\boldsymbol{v_n} = [u_n, w_n]^T$ (Figs. 2 and 3) in local axes (X_n, Z_n) through a kinematic transformation. This important kinematic transformation is schematically shown in Fig. 4 and is given by the following:

$$\begin{bmatrix} u_x^n \\ w_z^n \end{bmatrix} = \begin{bmatrix} \cos(\alpha_n) & \sin(\alpha_n) \\ -\sin(\alpha_n) & \cos(\alpha_n) \end{bmatrix} \cdot \begin{bmatrix} u_n \\ w_n \end{bmatrix} + \begin{bmatrix} \sin(\alpha_n) & \sin(\tilde{\alpha}_n) \\ \cos(\alpha_n) - 1 & \cos(\tilde{\alpha}_n) - 1 \end{bmatrix} \begin{bmatrix} t_r \\ t_s \end{bmatrix} \tag{4a}$$

Eq. (4a) can be written in more simple terms by renaming vectors and matrixes as follows:

$$\boldsymbol{v_g^n} = \boldsymbol{R_n^T v_n} + \boldsymbol{r_n} t_r + \boldsymbol{s_n} t_s \tag{4b}$$

where subscript "g" denotes a vector in global axes ($X - Z$), subscript "n" (or k, with $k = 1, \ldots, n$) denotes a vector in local axes ($X_n - Z_n$), and superscript "n" denotes the contribution of the n-th rubber layer. The kinematic vectors $\boldsymbol{r_n}$ and $\boldsymbol{s_n}$ allow to consider the contribution of the rigid body rotation of the n-th rubber layer and steel shim, respectively.

The steel shims immediately above the n-th rubber layer have a rigid-body translation and rotation, and its rotation $\tilde{\alpha}_n$ is identical to the rotation of the upper face of the rubber layer in contact with it. The vector of local internal forces, $\boldsymbol{p_n} = [V_n, P_n]^T$, relates to the vector of external forces acting on the isolator, $\boldsymbol{p_t} = [V_x, P_z]^T$, by the transpose of the above rotation matrix, $\boldsymbol{R_n}$ (Eqs. (4a) and (4b)), i.e.

$$\boldsymbol{p_n} = \boldsymbol{R}_n \boldsymbol{p_t} \tag{5}$$

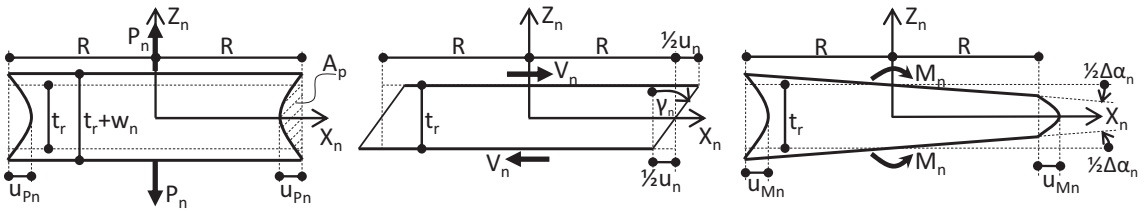

Fig. 3. Local forces and displacement parameters: (a) axial load and normal displacement (and rubber bulging); (b) shear load and angular deformation (shear distortion); and (c) bending moment and rotation (and rubber bulging).

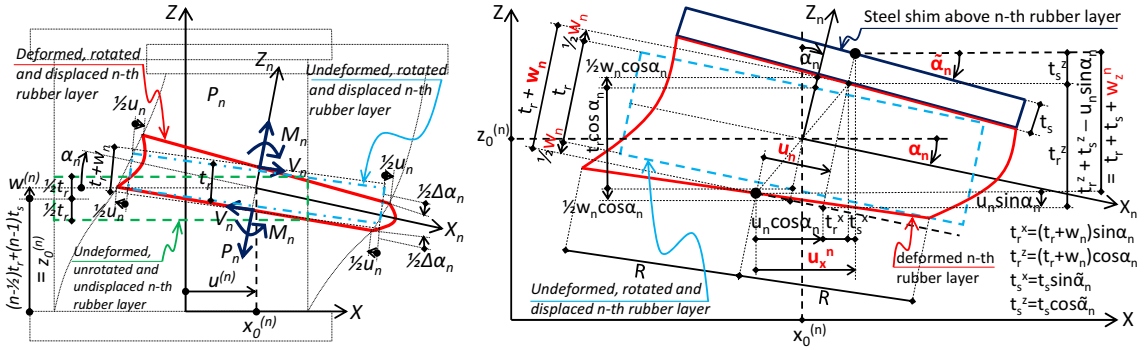

Fig. 4. Kinematics of the n-th rubber layer in the deformed configuration: (a) n-th rubber layer within the isolator; (b) n-th rubber layer and upper steel shim.

2.4. Translation of the local axes due to large shear deformations and rotation

The vector of global displacement at the centroidal plane of the n-th rubber layer, $\boldsymbol{v}_g^{(n)} = [u^{(n)}, w^{(n)}]^T$ (Fig. 4(a)), can be obtained by summing the contributions of all $(n-1)$ rubber layers and steel shims below (Eq. (4b)), leading to the following:

$$\boldsymbol{v}_g^{(n)} = \sum_{k=1}^{n-1}\begin{bmatrix} u_k\cos\alpha_k + w_k\sin\alpha_k + t_r\sin\alpha_k + t_s\sin\tilde{\alpha}_k \\ -u_k\sin\alpha_k + w_k\cos\alpha_k - t_r(1-\cos\alpha_k) - t_s(1-\cos\tilde{\alpha}_k)\end{bmatrix} + \frac{1}{2}\begin{bmatrix} u_n\cos\alpha_n + w_n\sin\alpha_n + t_r\sin\alpha_n \\ -u_n\sin\alpha_n + w_n\cos\alpha_n - t_r(1-\cos\alpha_n)\end{bmatrix} \tag{6a}$$

The above equation, can be rewritten in matrix form as follows:

$$\begin{aligned}\boldsymbol{v}_g^{(n)} &= \sum_{k=1}^{n-1}\boldsymbol{R}_k^T\boldsymbol{v}_k + \frac{1}{2}\boldsymbol{R}_n^T\boldsymbol{v}_n + \underbrace{\sum_{k=1}^{n-1}\boldsymbol{r}_k}_{=\bar{\boldsymbol{r}}_{n-1}}t_r + \frac{1}{2}\boldsymbol{r}_n t_r + \underbrace{\sum_{k=1}^{n-1}\boldsymbol{S}_k}_{=\bar{\boldsymbol{s}}_{n-1}}t_s \\ &= \sum_{k=1}^{n-1}\boldsymbol{R}_k^T\boldsymbol{v}_k + \frac{1}{2}\boldsymbol{R}_n^T\boldsymbol{v}_n + \left(\bar{\boldsymbol{r}}_{n-1} + \frac{1}{2}\boldsymbol{r}_n\right)t_r + \bar{\boldsymbol{s}}_{n-1}t_s\end{aligned} \tag{6b}$$

Eq. (6b) can also be written in terms of the vector of global forces, $\boldsymbol{p}_t = [V_x, P_z]^T$, using the local force-displacement relationship given by Eq. (3), i.e.

$$\boldsymbol{v}_n = \boldsymbol{F}\boldsymbol{R}_n\boldsymbol{p}_t \tag{7}$$

Combination of Eqs. (6b) and (7), leads to

$$\begin{aligned}\boldsymbol{v}_g^{(n)} &= \underbrace{\sum_{k=1}^{n-1}\overbrace{\boldsymbol{R}_k^T\boldsymbol{F}\boldsymbol{R}_k}^{=\boldsymbol{F}_k}}_{=\bar{\boldsymbol{F}}_{n-1}}\boldsymbol{p}_t + \frac{1}{2}\overbrace{\boldsymbol{R}_n^T\boldsymbol{F}\boldsymbol{R}_n}^{=\boldsymbol{F}_n}\boldsymbol{p}_t + \left(\bar{\boldsymbol{r}}_{n-1} + \frac{1}{2}\boldsymbol{r}_n\right)t_r + \bar{\boldsymbol{s}}_{n-1}t_s \\ &= \left(\bar{\boldsymbol{F}}_{n-1} + \frac{1}{2}\boldsymbol{F}_n\right)\boldsymbol{p}_t + \left(\bar{\boldsymbol{r}}_{n-1} + \frac{1}{2}\boldsymbol{r}_n\right)t_r + \bar{\boldsymbol{s}}_{n-1}t_s\end{aligned} \tag{8}$$

Adding into Eq. (8) the undeformed position of the centroid of the n-th rubber layer, the vector of global coordinates of the origin of the local axes, $\boldsymbol{r}_g^{(n)} = [x_o^{(n)}, z_o^{(n)}]^T$ (Fig. 3) for the n-th rubber layer results in

$$\boldsymbol{r}_g^{(n)} = \begin{bmatrix} x_o^{(n)} \\ z_o^{(n)}\end{bmatrix} = \begin{bmatrix} 0 \\ \frac{1}{2}(2n-1)t_r + (n-1)t_s\end{bmatrix} + \begin{bmatrix} u^{(n)} \\ w^{(n)}\end{bmatrix} = \boldsymbol{r}_0^{(n)} + \boldsymbol{v}_g^{(n)} \tag{9}$$

2.5. Global force-displacement relationship of the isolator

In the global force-displacement of the isolator represented in Fig. 2, each rubber layer provides a stiffness associated with local shear forces, i.e. k_h, k_v, and k_α for the shear, axial, and bending stiffnesses. Those stiffnesses are implicit in Eqs. (1)–(3). In addition to the four hypotheses mentioned earlier in Section 2.1, the following extra assumptions are considered: (1) the convention for the positive directions for shear, axial, and bending (and the corresponding displacements and rotation) is that of a positive face (axis coming out of the plane, or upper face), that is to the right (shear), up (tension) and clock-wise (bending). The opposite occurs on lower (negative face) as shown in Fig. 4(a); (2) to calculate $\Delta\alpha_n$, which is necessary to define the kinematic matrix $\boldsymbol{R}_n$, the internal bending moment across the rubber layer, M_n, was assumed as stated earlier approximately constant within the rubber layer and is computed at the mid-plane of the layer. This internal bending moment corresponds to Eq. (14) next, at the global deformed coordinate $z = z_o^{(n)}$ (Eq. (9)), which corresponds to the local coordinate $z_n = 0$.

Considering isolator shown in Fig. 5 and the loads acting in the positive sense as defined above, the equilibrium leads to

$$M_y^H - M_y^0 - P_z u_x + V_x(H + w_z) = 0 \tag{10}$$

Because of the end constrains, the magnitude of the bending moment at the base (M_y^0) and at the top of the isolator (M_y^H) is equal but with opposite sign ($M_y^0 = -M_y^H$), and then

$$M_y^H - M_y^0 = 2M_y^H = -2M_y^0 = P_z u_x - V_x(H + w_z) \tag{11}$$

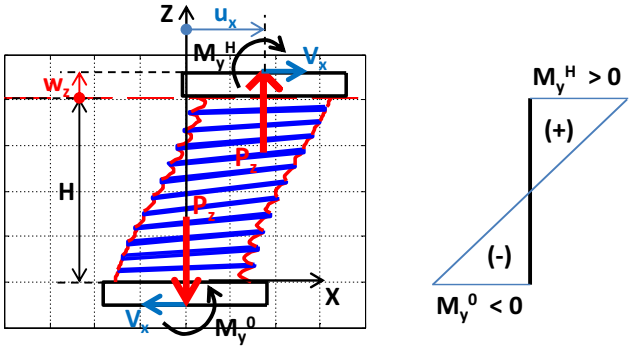

Fig. 5. Schematic view of the complete isolator equilibrium: (a) isolator deformed by axial and shear forces, and bending moment; (b) bending moment diagram, not a linear function.

Solving for the bending moment at the base

$$M_y^0 = \frac{1}{2}(V_x(H + w_z) - P_z u_x) \tag{12}$$

Consider a segment of the isolator, ranging from the base up to the mid-plane of the n-th rubber layer. In the centroid of area of that mid-plane, whose vector of deformed global coordinates is $\boldsymbol{r}_g^{(n)} = [x_o^{(n)}, z_o^{(n)}]^T$, the internal resulting loads in global axes are V_x, P_z, $M_y = M_n$. Therefore, the static equilibrium requires that

$$V_x z_o^{(n)} - P_z x_o^{(n)} + M_n - M_y^0 = 0 \tag{13}$$

Combining Eqs. (12) and (13), the internal bending moment at the mid plane of the n-th rubber layer is

$$M_n = V_x\left(\frac{1}{2}(H + w_z) - z_o^{(n)}\right) - P_z\left(\frac{1}{2}u_x - x_o^{(n)}\right) \tag{14}$$

By knowing the internal bending moment M_n, the relative rotation of any rubber layer, $\Delta\alpha_n$, can be calculated using Eq. (2). Then, the absolute rotations α_n and $\tilde{\alpha}_n$ for the n-th rubber layer can be computed as follows:

$$\alpha_n = \frac{1}{2}\Delta\alpha_n + \sum_{k=1}^{n-1}\Delta\alpha_k; \quad \tilde{\alpha}_n = \alpha_n + \frac{1}{2}\Delta\alpha_n = \sum_{k=1}^{n}\Delta\alpha_k \tag{15}$$

With these rotations, the kinematic matrix $\boldsymbol{R_n} = \boldsymbol{R_n}(\alpha_n)$ and vectors $\boldsymbol{r_n} = \boldsymbol{r_n}(\alpha_n)$, with $n = 1, \ldots, N$, and $\boldsymbol{s_n} = \boldsymbol{s_n}(\tilde{\alpha}_n)$, with $n = 1, \ldots, N-1$, can be determined by Eq. (4). Using $\boldsymbol{R_n}$, the local shear and axial forces, $\boldsymbol{p_n} = [V_n, P_n]^T$, are given in terms of the external axial and shear forces, $\boldsymbol{p_t} = [V_x, P_z]^T$ using Eq. (5). Finally, the global displacements on top of the isolator $\boldsymbol{v_t} = [u_x, w_x]^T$, can be expressed in terms of the global forces $\boldsymbol{p_t} = [V_x, P_z]^T$ by

$$\begin{aligned}\boldsymbol{v_t} &= \underbrace{\sum_{k=1}^{N}\boldsymbol{R}_k\boldsymbol{F}\boldsymbol{R}_k^T}_{=\bar{\boldsymbol{F}}_N}\boldsymbol{p_t} + \underbrace{\sum_{k=1}^{N}\boldsymbol{r_n}}_{=\bar{\boldsymbol{r}}_N}t_r + \underbrace{\sum_{k=1}^{N-1}\boldsymbol{s_n}}_{=\bar{\boldsymbol{s}}_{N-1}}t_s \\ &= \bar{\boldsymbol{F}}_N\boldsymbol{p}_t + \bar{\boldsymbol{r}}_N t_r + \bar{\boldsymbol{s}}_{N-1}t_s\end{aligned} \tag{16a}$$

Inversion of this matrix relationship given leads to

$$\boldsymbol{p_t} = \bar{\boldsymbol{F}}_N^{-1}(\boldsymbol{v_t} - \bar{\boldsymbol{r}}_N t_r - \bar{\boldsymbol{s}}_{N-1}t_s) \tag{16b}$$

Eqs. (16a) and (16b) rule the relation between geometric parameters, loads and displacement of the model shown in Fig. 2.

2.6. Numerical algorithm to solve the problem

The algorithm presented here allows to determine the external forces ($\boldsymbol{p_t}$) by knowing the global displacements ($\boldsymbol{v_t}$). The iterative procedure proposed herein requires an initial guess for the external global forces ($\boldsymbol{p_t}^{(0)}$) acting on the isolator, related with the known displacements ($\boldsymbol{v_t}$). Fewer iterations are required if the nonlinearity is low ($|u_x/H_r| \ll 1$) and if the initial approximation of the global forces ($\boldsymbol{p_t}^{(0)}$) is adequate. The procedure is described next step by step:

1. Estimate $\boldsymbol{p_t}^{(0)}$. If a better initial approximation of forces $\boldsymbol{p_t}^{(0)} = [V_x^{(0)} \quad P_z^{(0)}]^T$ is not available, an estimate can be obtained by using the displacement known $\boldsymbol{v_t} = [u_x, w_z]^T$ and the linear decoupled relationship, $\boldsymbol{p_t}^{(0)} = \boldsymbol{F}^{-1}\boldsymbol{v_t}$. Alternatively, a nonlinear explicit method can be used to get that initial approximation as for the two-spring model.
2. Use $\boldsymbol{p_t}^{(0)}$ in Eq. (8) to compute $\boldsymbol{v_g}^{(n)}$; then, replace this in Eq. (9) to obtain $\boldsymbol{r_g}^{(n)}$. With the above, and using Eq. (14) calculate M_n, for $n = 1, \ldots, N$. Finally, with M_n determine the rotations $\Delta\alpha_n$, α_n and $\tilde{\alpha}_n$ using Eqs. (2) and (15).
3. Compute a first estimation of the kinematics matrix and vectors $\boldsymbol{R_n}^{(1)}$, $\boldsymbol{r_n}^{(1)}$ and $\boldsymbol{s_n}^{(1)}$ by replacing α_n and $\tilde{\alpha}_n$ in Eq. (4). Replace the above and $\boldsymbol{v_t}$ in Eq. (16b) to calculate the first iteration of the vector of global loads $\boldsymbol{p_t}^{(1)}$.
4. Use $\boldsymbol{p_t}^{(0)}$ and $\boldsymbol{p_t}^{(1)}$ to calculate a parameter of error; this can be defined by $\boldsymbol{e} = \|\boldsymbol{p_t}^{(1)} - \boldsymbol{p_t}^{(0)}\|/\|\boldsymbol{p_t}^{(1)}\|$. Obviously, if $\|\boldsymbol{p_t}^{(1)}\| = 0$, there is no nonlinearity, and then $\boldsymbol{e} = \boldsymbol{0}$, which corresponds to the force $\boldsymbol{p_t} = [0, 0]^T$.
5. Repeat the procedure (2) to (4) above until the iteration error is lower than a prescribed tolerance.

The above algorithm can be used to obtain the static response of an isolator considering the geometric nonlinearity due to large lateral displacements. However, the same algorithm can also be used in a response-history analysis. To do this soon, and in order to reduce the number of iterations, the initial global forces can be considered equal to the loads at the previous integration time instant. Next, numerical results are presented that validate the procedure and algorithm presented here.

3. Model results

Although the model could be applied to a large number of different cases, results show similar general trends. Therefore, a single isolator has been included herein to demonstrate the response of a circular multilayer elastomeric isolator. The specimen whose response is shown in Figs. 6–9 has radius R = 30 cm, N = 40 rubber layers of thickness t_r = 12 mm, steel shims of thickness t_s = 3 mm and nominal shear modulus G = 7.5 kg/cm^2, all values commonly used in building design [12,20]. The rubber was considered as an incompressible material in the results shown in Sections 3.1 and 3.2. In Sections 3.3 and 3.4, a compressible material was assumed, with a Bulk modulus K = 20.000 kg/cm^2 for rubber [1]. Fig. 7 shows results for different values of t_r, t_s and N used to obtain isolators with different shape factors S, but with the same total rubber height (H_r = 480 mm) and total steel height (H_s = 120 - mm). These values were used to analyze the sensitivity of the effective stiffness of the isolator relative to the shape factor S. In the results presented next, all loads are normalized with respect to the critical buckling load P_{cr} obtained using the well-known two-spring isolator model [5,10,12].

3.1. Global behavior

Model results (MSM) in terms of force-displacement curves are shown in Fig. 6 and curves for stiffness reduction in Fig. 7. Equivalent results obtained by the two-spring model (TSM) [5,10,12] and

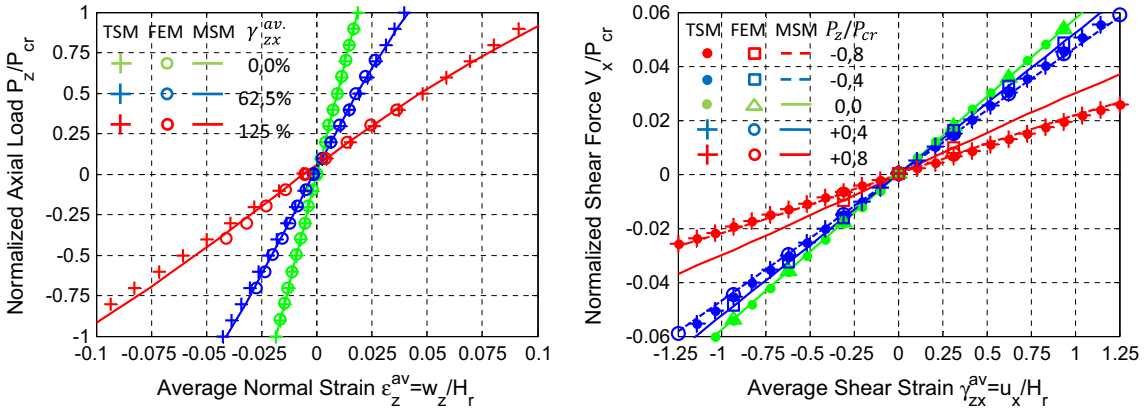

Fig. 6. Comparison of results using TSM, FEM and MSM: (a) axial load versus vertical displacement as a function of lateral displacement (compression $P_z < 0$ and tension $P_z > 0$); and (b) shear load versus lateral displacement as a function of P_z/P_{cr}.

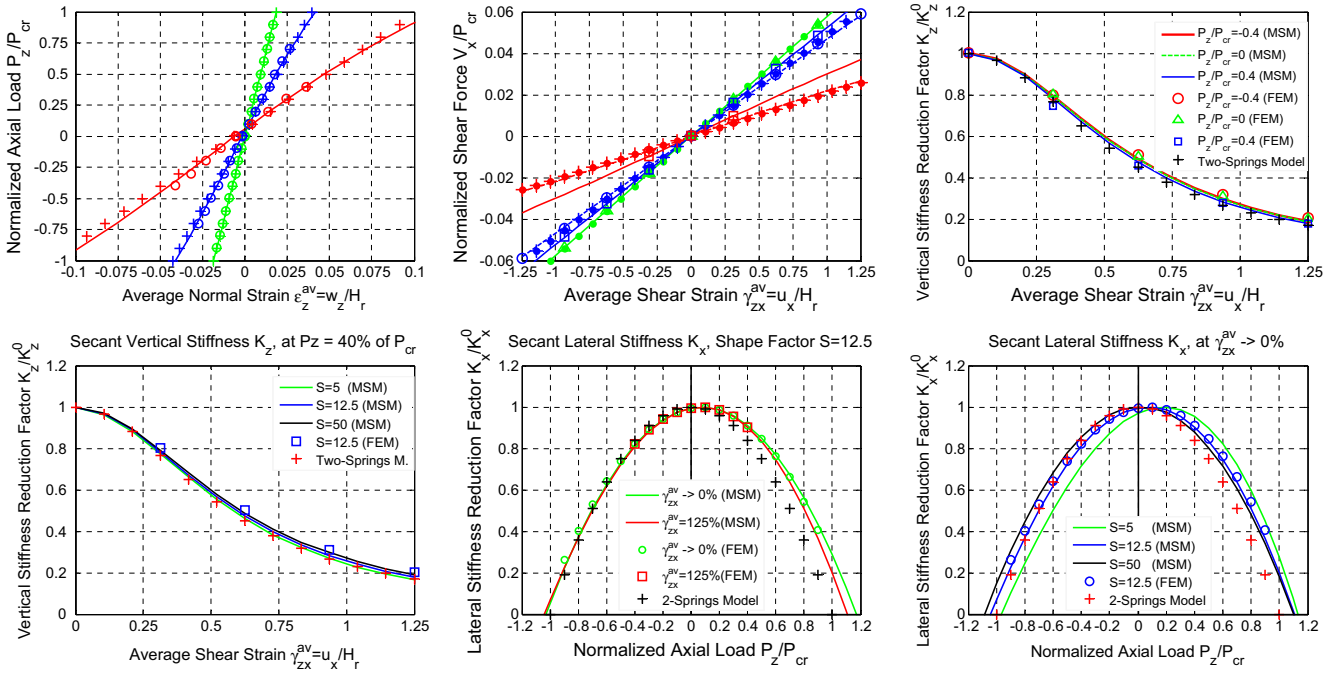

Fig. 7. Stiffness reductions in a circular isolator with different shape factors: (a) vertical stiffness reduction factor as a function of lateral displacement; and (b) horizontal stiffness reduction factor as a function of P_z/P_{cr}.

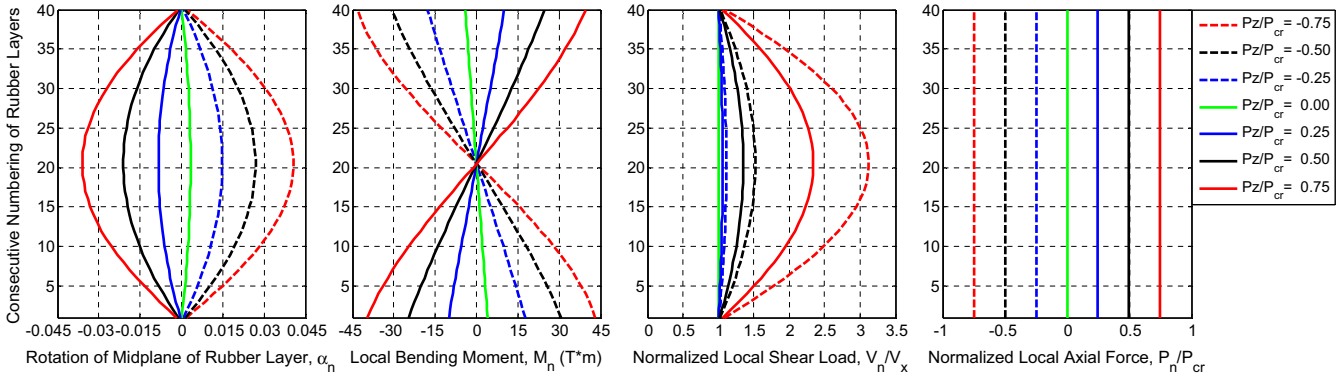

Fig. 8. Internal response of a circular isolator, for several axial loads, considering $u_x = 30$ cm: (a) rotation of the mid-plane of each rubber layer; (b) bending moment; (c) normalized local shear forces; and (d) normalized axial forces.

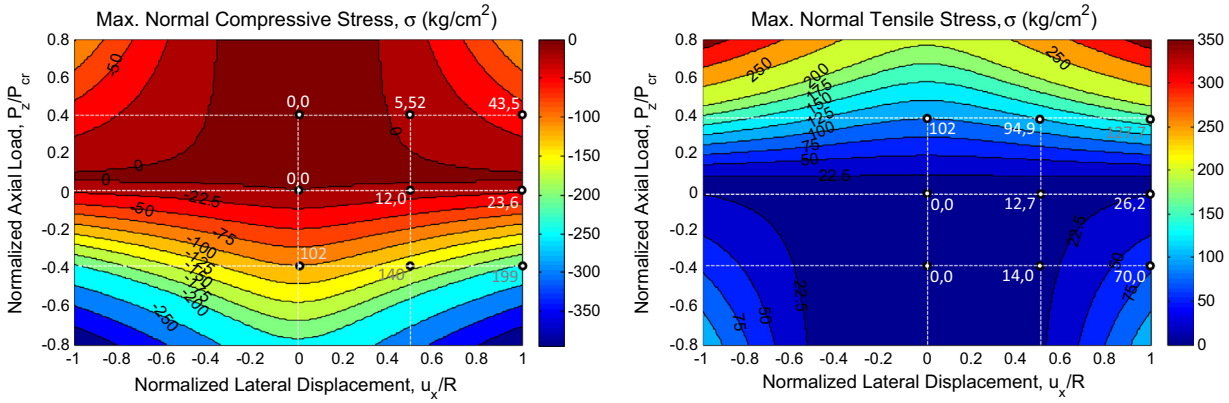

Fig. 9. Maximum stresses at lowest rubber layer: (a) peak normal compressive stress; (b) peak normal tensile stress.

a finite element model (FEM) of the isolator developed in the software COMSOL Multiphysics 5.0© [21] are presented in the same figures.

Fig. 6(a) shows that results for the three models are quite consistent. Please notice that only the curve corresponding to $u_x = 0$ crosses the origin; the other curves intersect the vertical axis at a point slightly above the origin. This means that under the presence of lateral displacement, an axial tensile load is required to maintain the vertical displacement equal to zero. Such is the case because the lateral displacement generates a rotation of the rubber layers, and hence both global loads (V_x and P_z) have non-zero projections along both local axes ($X_n - Z_n$). Alternatively, this implies that a pure global shear force produces a vertical global displacement $w_z < 0$ without an axial load. In Fig. 6(b) results show that the proposed MSM and TSM predict closer results in compression than in tension. This is because the TSM is not capable of reproducing any differences in the behavior of the isolator under compression or tension, by which crosses (compression) and points (tension) are overlaid. However, the FEM used is capable of reproducing the different behavior in compression (squares) and tension (circles), as it does the MSM. In both cases, the results obtained by the FEM and the MSM are very similar.

The curves of reduction of vertical stiffness with increasing lateral displacement (Fig. 7(a)) are similar for the TSM, the FEM, and the MSM. However, results of the MSM match better the FEM results than the TSM ones. Besides, results of the MSM and the FEM show slightly higher vertical stiffness values than those of the TSM. Values of the reduction in lateral stiffness with larger axial load (Fig. 7(b)) obtained using the MSM and TSM become closer as the shape factor S grows. However, the sensitivity of these curves with S is low when its value is higher than 10, which is common in real building design [12]. Furthermore, using the MSM the critical buckling load reached in tension is higher than in compression, especially when S is low; these loads tend to be similar as S increases.

Unlike the TSM for which the lateral stiffness is symmetric relative to axial load with a maximum value at $P_z = 0$, the MSM and the FEM show that the lateral stiffness reaches a maximum with a small (as compared with the buckling load) tensile load. The above is explained because a lateral displacement of the isolator generates rotation of the rubber layers that goes in the opposite direction as the one generated by the tensile load. Indeed, there is an axial tensile load which magnitude is capable of canceling the rotation of the rubber layers produced by the shear force. For that exact axial tensile force, all rubber layers of the isolator remain horizontal. Therefore, the lateral displacement is exclusively generated by shear and the behavior of the isolator coincides with that of the uncoupled case. Any different axial load will cause a reduction in lateral stiffness as compared to the uncoupled force condition. For example, in the case of $S = 12.5$, the critical buckling load reached in compression (Fig. 7(b)) by using the MSM is 3.6% larger than that obtained using the TSM. However, in tension, the critical buckling load of the MSM differs from the TSM load by 10.9% (Fig. 7(b)). In the latter case, the maximum lateral stiffness obtained from the results of the MSM and the FEM are reached for an axial load, Ps, approximately equal to 8% of the critical buckling load. These results, which carry over to other isolator geometries, imply that the MSM is capable of reproducing the non-linear geometric behavior of the isolator.

3.2. Internal behavior

Although it is true that the internal forces of the isolator may be obtained by the stress-strain state in the isolator, unlike other models [10,5,4,13–15], the MSM can characterize explicitly and directly the stress and strain of each rubber layer in terms of local loads and displacements. This is achieved by means of the solutions of the differential equations that govern the behavior of a single rubber layer subjected to axial load and bending moment [1]. The results are illustrated in Figs. 8 and 9.

Although all curves in Fig. 8(a) are approximately equally spaced, the curve corresponding to $P_z = 0$ is not vertical but shifted to the right, which indicates that shear force does generate rotation of the cross section. These rotations occur in the same direction of the lateral displacement, i.e. clockwise if the lateral displacement is along axis X and vice versa. Moreover, the curves corresponding to a compressive axial load imply higher rotations than those associated with the same magnitude of tensile load. This is because the compressive axial force generates a rotation that adds to the rotation generated by lateral displacement. On the other hand, a tensile axial force produces rotations in the opposite direction to those generated by the lateral displacement. A similar condition occurs with the internal bending moment curves (Fig. 8(b)) since M_n is proportional to $\Delta\alpha_n$, which is related to the slope of the absolute rotation α_n (Fig. 8(a)).

The magnitude of the shear force (Fig. 8(c)) along the local axis X_n corresponds to the projection of the global shear and axial force. If the absolute rotation α_n is zero, the shear force in local axis is equal to the global shear force in every rubber layer. Under the presence of non-zero rotation α_n, the local shear force is amplified by the presence of axial force (tension or compression). Because a compression load causes rotation α_n, which adds to that generated by the lateral displacement, the local shear load is increased more significantly by a compressive load than by an equal magnitude tensile load (Fig. 8(c)). Consequently, the theoretical lateral instability due to axial load (buckling load) is reached earlier in

compression than in tension (Fig. 7(b)). This does not mean in practice that buckling in tension occurs for a higher axial load since buckling in tension is preceded by cavitation.

It is apparent from the figure that the local axial forces along the high of the isolator are practically constant for all rubber layers (Fig. 8(d)), and equal to the global axial force. This is the result of a small contribution of the external shear, since rotations α_n are very small and external shear load is commonly one order of magnitude smaller than the external axial force.

Using the MSM, the normal stresses inside the rubber and along the entire isolator were calculated in many points and for many combinations of axial force and lateral displacement. As it should be, the maximum stresses always occur at the bottom and top rubber layers. The maximum normal stress in the rubber, obtained for the elastomeric isolator described at the beginning of Section 3 is shown in Fig. 9. The results shown are symmetrical with respect to the vertical axis ($u_x = 0$), which is expected due to the symmetry of the problem. However, these results are not symmetrical with respect to the horizontal axis ($P_z = 0$), which is not the case with the results obtained with the TSM [12].

It must be emphasized that although Fig. 8(b) shows high tensile stress results, this does not mean that the isolator be able to achieve those levels of tension load. Before reaching those high tensile stresses, the rubber will fail due to cavitation. The cavitation stress in rubber is approximately constant for rubber layers with small thickness and it is proportional to the modulus of elasticity [22]. This tensile cavitation stress is about $3G$ [6], which corresponds to 22.5 kg/cm^2 for the example shown. In Fig. 9(b), the contour curve associated with this cavitation stress corresponds to a plateau that is reached at a load of about 10% of the critical buckling load P_{cr}, even in the case of large lateral displacements ($u_x = \pm R$). In contrast, the same stress in compression (Fig. 9(a)) is reached with the same compressive load, but it only requires a small lateral displacement, $|u_x| \ll$ R, whereas for $u_x \approx \pm R$, the same stress can be reached without axial load. This result suggests that is possible to resist a value of axial tensile load of about 10% of the P_{cr} on the elastomeric isolator prior to cavitation in the rubber.

3.3. Comparison with experimental results

The proposed MSM aims to characterize the nonlinear geometric behavior of the isolator. Therefore, experimental data of elastomeric isolators without leading a core and with low damping ratio were preferred in order to validate the results of the model. It was found in the literature an experimental study of a group of rubber bearing isolators subjected to large lateral displacement and high axial loads [8]. In the study, curves considering the effect of axial load in the reduction of lateral stiffness were obtained for shear force versus lateral displacement. Furthermore, the critical buckling loads for different levels of lateral displacement were also determined. This study is the best possible reference available for comparison between analytical and experimental results, and thus validates the MSM presented herein. In this experimental study, all bearings had bolted connections at the top and bottom to prevent rollover. As it was assumed in the MSM, bearings could not rotate at their ends. From this experimental study, the bearing series 300 was selected to compare with the results obtained from the MSM. This series corresponds to square isolators with shape factor $S = 5$, number of rubber layers $N = 8$, thickness $t_r = 0.25$ in., thickness of steel shims $t_s = 0.055$ in., cross section of 5 by 5 in., and total height $H = 4.385$ in.

The study indicates that the shear moduli at $\gamma = 0$ and $\gamma = 1$ were $G_0 = 0.200$ kip/in^2 and $G_1 = 0.136$ kip/in^2, respectively [8]. The dependence of shear modulus with shear strain was calibrated using a function $G = G_0 - (G_0 - G_1)\,\gamma^C$. Independent of the value of parameter C, the above function satisfies the conditions at $\gamma = 0$ and $\gamma = 1$. Parameter C must be constrained to be larger than zero, since the shear modulus, G, is a decreasing function of the shear strain γ according vast experimental data. To determine C, the error between the responses of the MSM as compared with the experimental results was minimized, considering a set of values of C from 0.05 to 1 with step 0.005; the optimal value obtained was C = 0.50.

Using this function for the shear modulus, the results of the MSM were calculated, considering a Bulk modulus $K = 20.000$ kg/cm^2 as a typical value for rubber [1]. Then, numerical results were compared with the experimental data in Fig. 10. In this figure, the units used in the experimental study [8], kips and inches, have been maintained for comparison reasons. These units are exclusively valid for Fig. 10.

In spite of several uncertainties, the data shown in Fig. 10 present a relatively good correlation between experimental and analytical results. The differences observed may be due to several reasons, for instance, the eventual inelastic behavior of the rubber compound used in the experiments. Even if the rubber in the isolator selected has low damping, such damping may influence the forces measured. The load path followed could also influence the results. Indeed, by observing the left plot of Fig. 10, to obtain the experimental critical buckling load as a function of lateral displacement, an axial load was imposed first and then the lateral displacement was increased until reaching instability. On the other hand, in the right plot of Fig. 10, the experimental procedure consisted in imposing a lateral displacement, and then increasing the axial load until reaching a specified value, and measuring the shear force in the equilibrium condition. In the two previous cases, because different paths were followed to reach the equilibrium, any path dependency would lead to different equilibrium conditions. In fact, for the experimental results shown in the right plot of Fig. 10 for

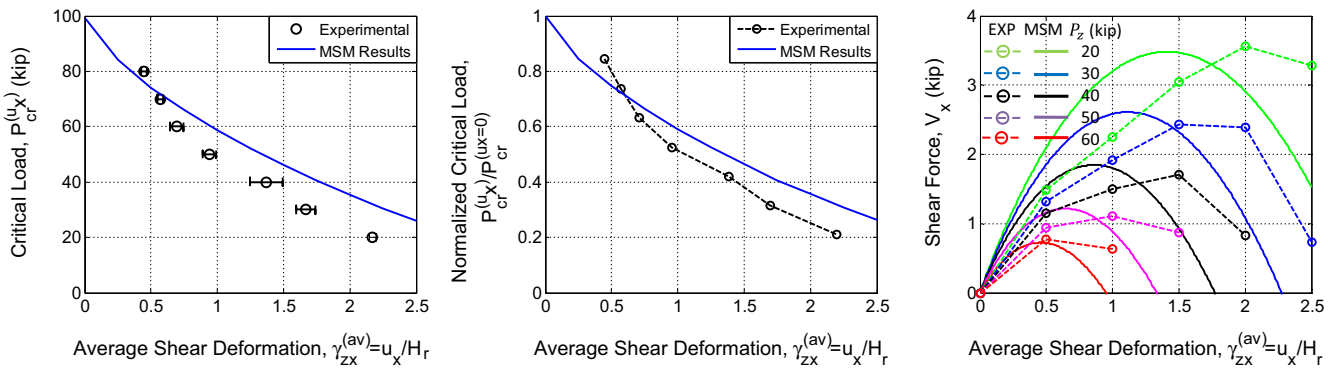

Fig. 10. Comparison of experimental results (from [8]) and analytical results obtained using the MSM.

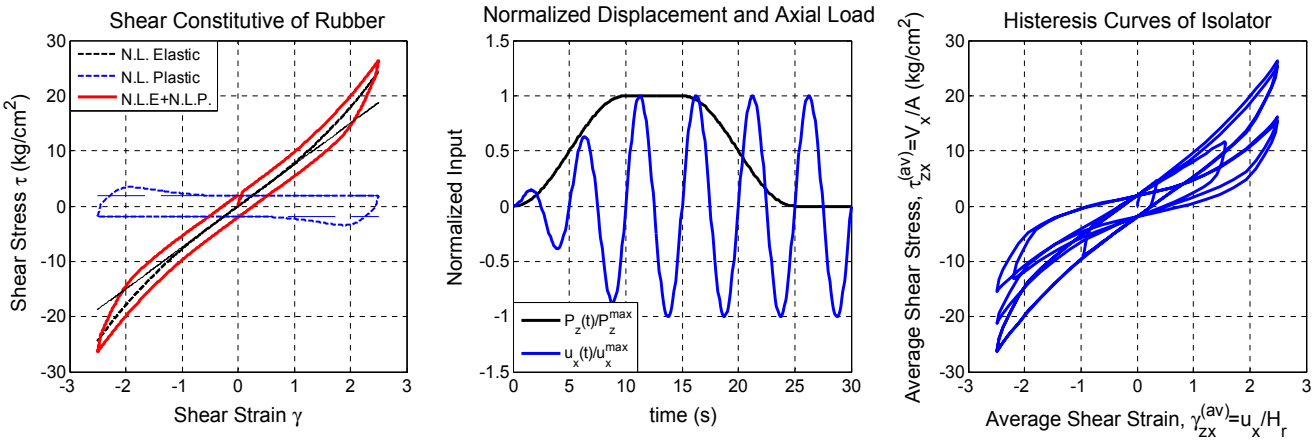

Fig. 11. Inelastic model for rubber: (a) plastic and nonlinear elastic stress-strain constitutive behavior of rubber; (b) imposed normalized axial load and lateral displacement– $u_x^{max} = 2.5H_r$ and $P_z^{max} = 0.8P_{cr0}^{(MSM)}$; (c) complete hysteresis curves of the isolator for the input defined in (b) using the model shown in (a) plus the MSM.

axial loads P_z = 40, 50 and 60 kip it is possible to estimate the shear strain which leads to zero lateral stiffness. For P_z = 40 kip, such shear strain is between 2 and 2.5; for P_z = 50 kip the strain is between 1.5 and 2, and for P_z = 60 kip it is between 1 and 1.5. By observing now the left plot in Fig. 10, the shear deformation corresponding to buckling loads equal to 40, 50 and 60 kips can be estimated as 1.37, 0.94 and 0.69, respectively. These results confirm the hypothesis that the inelastic component is not negligible in the experimental response presented. Nevertheless, the proposed MSM is able to capture the experimental trends observed.

3.4. Implementation of the MSM for response-history analysis

The use of the proposed MSM in a response history analysis of a 30-story building subjected to the N00°E and vertical component of the Sylmar seismic record (1994) is presented. The simplified analysis performed was planar and considered a model of a building with flexible columns and infinitely stiff beams. The isolation system consists of tree circular rubber bearing isolators under the columns, and the isolators have 40 equal rubber layers of thickness t_r = 5 mm, steel shims t_s = 2 mm, and shape factor S = 33. Two models of the isolators were considered: (1) the TSM [5,10,12]; and (2) the MSM proposed here. For both cases, the inelastic behavior of the rubber was added by an element working in parallel with the nonlinear geometric model described earlier. The inelastic behavior of the isolator was characterized by the well-known Bouc-Wen differential equation [23].

In order to include elastic hardening in the rubber, a shear stress-strain curve was defined by the authors based on physical parameters of the mechanical behavior of the rubber:

$$\tau_{NLE} = G_0\gamma\left(1 + \left(\frac{G_M - G_0}{G_0}\right)\left(\frac{1+\text{sign}(|\gamma| - \gamma_H)}{2}\right)\left(\frac{|\gamma| - \gamma_H}{\gamma_M - \gamma_H}\right)^{n_H}\right) \tag{17}$$

where τ_{NLE} is the nonlinear elastic stress, γ is the shear strain in rubber, γ_M is a shear strain for which the secant shear modulus of rubber is known ($G(\gamma_M) = G_M$), γ_H is a shear strain in rubber for which the hardening begins, G_0 is the shear modulus of rubber at $\gamma = 0$, G_M is the secant shear modulus of rubber at $\gamma = \gamma_M$, and $n_H > 1$ represents the gradual start of hardening—higher values of n_H represent a more gradual start of hardening.

In order to obtain a more realistic behavior, changes were made in the way of calculating the plastic strain τ_{NLP} using the Bouc-Wen state variable. These modifications include the following: (i) shear strain at yielding γ_y is defined as a function of the hardening in rubber; and (ii) shear stress of yielding τ_y is amplified in reversing the load if the rubber is in hardening zone.

$$f_H = 1 + \Delta f_H\left(\frac{\tau_{NLE}}{G_0\gamma} - 1\right)\left(\frac{1 - \text{sign}(z\cdot\gamma)}{2}\right), \text{ with } \gamma \neq 0 \tag{18a}$$

$$\gamma_y = \gamma_y^0 f_H^{n_y} \tag{18b}$$

$$\tau_{NLP} = (1-\alpha)G_0\gamma_y^0 z f_H \tag{18c}$$

where f_H is a factor related with the degree of hardening of rubber; Δf_H incorporates gradual growth of the factor f_H; γ_y^0 corresponds to the shear strain at the beginning of inelasticity of rubber in the range before hardening; $n_y > 1$ is related with the increase of inelastic shear strain in the zone of hardening; and z is the state variable of Bouc-Wen defined as in [23].

Since the purpose of this section is to show the use of the MSM in a response-history analysis, the physical parameters of rubber incorporated in Eqs. (17) and (18) were arbitrarily chosen as follows: $\gamma_y^0 = 0.05H_r$, $\gamma_H = 1$, $\gamma_M = 2.5$, $G_0 = 7.5$ kg/cm^2, $G_M = 9.75$ kg/cm^2, $n_H = 1.5$, $\Delta f_H = 5$ and $n_y = 1.5$. These values correspond to physically possible values for rubber. Using the above numbers, the resulting mechanical model is consistent with that experimentally found for rubber and is similar to a model used previously [4] as shown in Fig. 11.

Using the above plasticity model and hardening for the rubber, and superimposing that behavior to the TSM and the proposed MSM, the results shown in Figs. 12 and 13 were obtained. Fig. 12 shows that the response of the isolated structure using the TSM and MSM is very similar. The most significant differences are obtained in the base shear. The above suggests that for the purpose of designing a superstructure, the model used in characterizing the nonlinear behavior of the isolators seems to have limited influence. Also, Fig. 13 shows that the axial forces are very similar (see peak values), but the critical buckling load obtained using both models is somewhat different as seen by the corresponding proportion of the P_{cr0} in the maximum values. The critical buckling load for close-to-zero shear strain, P_{cr0}, calculated using the MSM (2,289 T) is greater than the one calculated using the TSM (2.114 T). However, MSM predicts a faster reduction of the buckling load with the increasing of lateral displacement and axial load than the TSM. This is because the MSM considers two aspects that the TSM does not take into account, i.e.: (1) the reduction of the effective area and inertia of each rubber layer due to the lateral displacement (overlapping area); and (2) the nonlinear variation of the internal

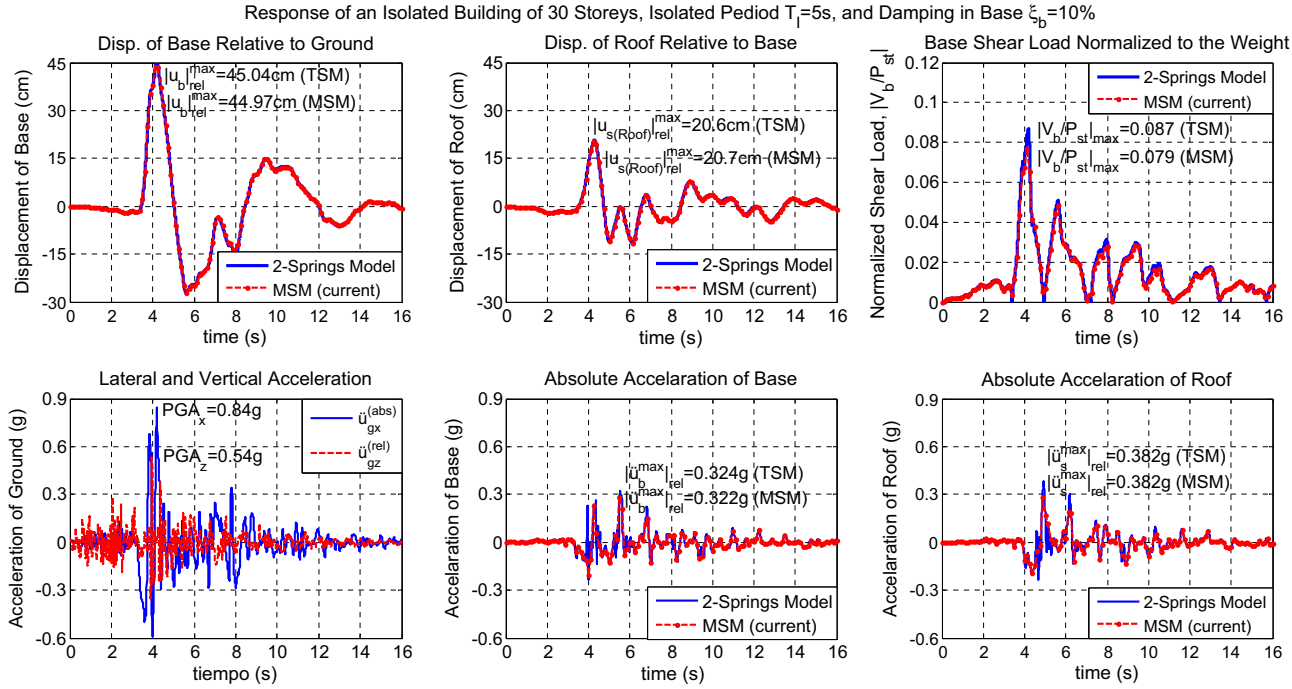

Fig. 12. Response history of the superstructure of a 30-story isolated building with $T_1 \approx 5$ s, and $\zeta_b \approx 10\%$.

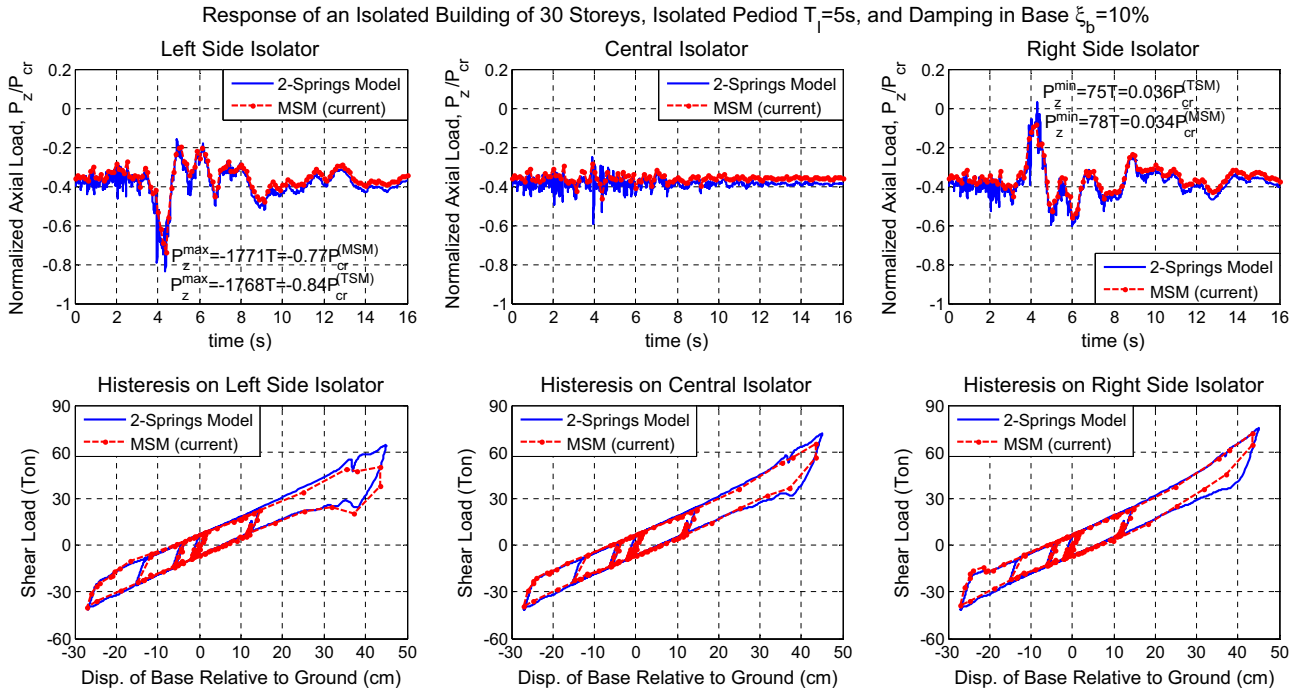

Fig. 13. Response history of the base for a 30-story isolated building with $T_1 \approx 5$ s, and $\zeta_b \approx 10\%$.

bending moment with height, which is aggravated with the increase in axial load (Fig. 8(b)). Consequently, both models provide similar results when lateral displacements and axial load are moderate ($|u_x|/H_r < 1$ and $P_z/P_{cr0} < 0.5$), but the results depart from each other when axial load and/or lateral displacement increases. The latter is reflected in the hysteresis curves of Fig. 13, which are quite similar between the TSM and the MSM with larger differences only for the maximum displacement cycle, which coincides with the maximum axial load.

4. Comparison with current models

In Table 1, the features of the proposed MSM are compared with some of the features of the existing models. The comparison includes some existing and desirable attributes, indicating whether each model has or has not the corresponding attribute. In order to reduce the amount of text in Table 1, a label is assigned to each model as follows: **M1**: Multi-springs model (MSM) based on a co-rotational formulation (proposed model); **M2**: Two-spring

Table 1
Comparative analysis between the MSM proposed and some of the currently existing models.

Model features	Model								
	M1	M2	M3	M4	M5	M6	M7	M8	M9
Reproduces the axial-lateral coupling in the load versus displacement relationship	Y	Y	Y	Y	Y	Y	Y[e]	Y[e]	Y[d]
Allows to determine the theoretical buckling load in compression and tension	Y	Y	Y	Y	Y	Y	N	N	N
Different buckling load under compression and tension	Y	Y	?[c]	Y	Y	?[c]	N	N	N
Leads to an element capable of being incorporated in a response-history analysis	Y	Y	Y	Y	Y	Y	N	N	N
How many degrees of freedom does the model have?	2	2	3N	2	2	3	2	2	3
Includes nonlinear hysteretic behavior ($\sigma_z = \sigma_z(\varepsilon_z, \varepsilon_z^{plastic})$) of the rubber within the model	Y	N	N	N	Y[d]	Y	N	Y	Y
Includes another hysteretic behavior like lead-core yielding	N	N	N	N	Y	Y	N	N	N
Could it include hysteretic behavior in each layer of rubber and not only as a global behavior of the isolator? [a]	Y	N	Y	N	N	N	N	N	N
Describes the asymmetry regarding axial load in tension and compression	Y	N	?[c]	Y[c]	N	?[c]	N	N	N
Allows characterizing the loads, moment, strain and stress within every rubber layer[b]	Y	N	Y	Y	N	N	N	N	N

[a] In order to properly include the hysteresis of the rubber in the model, the formulation must include it at the level of individual rubber layers. This is due to the fact that shear stresses are substantially different between central and top or bottom rubber layers when lateral displacement is large and axial load is moderate ($P_z/P_{cr} < 0.5$). However, a global hysteretic force is a good representation of hysteretic behavior when lateral displacement is not large ($|u_x|/H_r < 1$) and axial load is moderate.

[b] It is assumed that to achieve this, the model must be discrete and include each rubber layer or continuous throughout the isolator. A global characterization of the overall behavior of the isolator does not fulfill this attribute.

[c] According to the analytical formulation, it could be possible for the model to represent different behaviors under compression and tension forces; however, the authors only presented results in compression.

[d] The model presented includes hysteretic behavior of the lead core; however, this could be used to include the hysteresis of rubber, though the difference in shear load at each rubber layer would not be considered.

[e] Model only relates the vertical deformation with the axial load and lateral displacement.

model (TSM) according to Koh and Kelly, 1988 [10]; **M3**: Analytical 4×4 stiffness matrix for each rubber layer assembled to build the complete isolator according to Chang, 2002 [11]; **M4**: Isolator as a continuum element according to Kelly, 2003 [12]; **M5**: Two-spring model plus plastic lead core (TSML) according to Ryan et al., 2005 [5]; **M6**: Multi-spring model, two interior springs plus a bed of springs at the base and top, Yamamoto et al., 2009 [4]; **M7**: Model based on theory and concepts from experimentation that includes compression-shear coupling, Liu et al., 2009 [13]; **M8**: A variant of M7 describing tensile behavior and a bilinear stress-strain constitutive relationship for rubber, Yang et al., 2010 [14]; and **M9**: A variant of M7 incorporating the nonlinear behavior of rotation at the top of the isolator, He et al., 2012 [15].

As shown in Table 1, while the MSM can be improved, it already has several desirable attributes. In Section 3.4 a model for characterizing the inelastic behavior of the elastomeric material was presented; this model works in parallel with the non-linear geometric behavior characterized through the MSM. However, the MSM has the potential to include a hysteretic model for each individual rubber layer. Model M6 seems to be the most complete of all models, been capable of characterizing the geometric and material nonlinearities. Its performance has shown good correlation with experimental results even for high levels of shear strain (up 400%) and axial load close to the critical load, thus reproducing complex hysteretic behaviors [4]. However, most of the practical building designs are subject to axial load levels lower than 20% of the theoretical buckling load [5]. Indeed, many seismic isolation design codes limit the maximum allowed axial load on an elastomeric isolator to values lower than 50% of the buckling load. Additionally, in tall buildings where axial loads are higher, the isolation period required to achieve decoupling of the structure is also higher. The latter leads to isolators with larger rubber heights and hence less shear deformation. Therefore, in order for an isolator model to be practical for design purposes, it should have a reasonably good performance for mid to high strains, say about 150–200%, and axial loads less than 50% of the buckling load. Besides its larger simplicity and numerical efficiency, this is a requirement that the MSM proposed herein meets well.

5. Conclusions

The MSM proposed is based on a co-rotational formulation and shows consistent results with previous models and theories. Because it is constructed from the kinematics of the individual rubber layers, it also includes the possibility of incorporating more complex behaviors of the rubber material of layers. This is in addition to the advantage of computing specific details of the isolator response in terms of internal strains and stresses in each of the rubber layers. The results of the MSM were compared with those of the well-known TSM, with a finite element model, and with experimental data. Results show that the MSM predicts well the isolator response if compared with the TSM and finite element models, and reasonably well with experimental results.

The formulation presented, as well as the finite element model, proves that the common assumption of symmetry in the isolator behavior in tension and compression is incorrect. Indeed, for small axial loads in comparison with the theoretical buckling load ($P_z < 0.2P_{cr}$), these results demonstrate that the difference between the behavior in compression and tension increases with smaller shape factor S, say, less than 10. However, as the shape factor S increases, the difference in the behavior in tension and compression vanishes. The buckling load in tension is theoretically larger than in compression. This is explained by the fact that buckling occurs due to rotation of the cross section of the isolator. A compressive load always generates an extra rotation which adds to the one generated by the lateral load, while under tension this only occurs if the load exceeds a certain threshold of axial load (Ps). Hence, the theoretical buckling load in tension is higher than the one in compression, but it is never reached because of cavitation of the rubber.

The proposed model is able to characterize the global behavior of an isolator, its strain and stress field, and the deformations within each rubber layer. Therefore, it is possible to predict the peak strain and stress in each rubber layer, as well as the true deformed shape. This possibility also helps in dealing with manufacturing uncertainties in the geometric and mechanical properties of the isolator. Therefore, the MSM provides a simple methodology of propagating uncertainty from the isolator rubber layers into the properties of the global isolator. Another advantage of this methodology is the possibility to incorporate the inelastic behavior of rubber, which is immediate from this formulation.

Cavitation in rubber is supported by many experimental results and current models predict the theoretical tension force at which elastomeric isolators fail. This load is significantly smaller than the limit imposed by the cavitation forces experimentally observed. However, the proposed model shows results that are consistent with those experimentally observed.

A response history analysis was performed to illustrate the use of the MSM in a dynamic analysis framework. A model of inelasticity and hardening of rubber was incorporated into the model in order to reproduce the nonlinear behavior of the elastomer. The above model was implemented with the MSM and the TSM. Results of the response history analysis using both models show only slight differences, with larger discrepancies in the base shear. The analysis performed validates the MSM proposed and its capability to work in static and dynamic analyses including the inelastic and geometrically nonlinear behavior of the isolator. More importantly, the flexibility shown by the MSM in these examples is a proof that the methodology works well to model other layered isolator devices and materials. It also allows to propagate uncertainty from the level of layers to the level of the device.

Acknowledgments

This research has been sponsored by the National Science and Technology Council of Chile, CONICYT, under grant FONDECYT 1141187, and by the National Research Center for Integrated Natural Disaster Management CONICYT/FONDAP/15110017. The authors are grateful for this support and would like to thank also the insightful comments of the reviewers.

Appendix A. Supplementary material

Supplementary data associated with this article can be found, in the online version, at http://dx.doi.org/10.1016/j.engstruct.2016.09.055.

References

[1] Kelly JM. Earthquake-resistant design with rubber. Springer Verlag; 1997. http://dx.doi.org/10.100/978-1-4471-0971-6 [chapter 1, 1–18; chapter 7, 131–137, 141–148; chapter 8, 170–184].
[2] Naeim F. Design of seismic isolated structures: from theory to practice. John Wiley & Sons; 1999 [chapter 1, 1–24; chapter 5, 93–100; chapter 6, 121–133].
[3] Komuro T, Nishikawa Y, Kimura Y, Isshiki Y. Development and realization of base isolation system for high-rise buildings. J Adv Concr Technol 2005;3(2):233–9.
[4] Yamamoto S, Kikuchi M, Ueda M, Aiken ID. A mechanical model for elastomeric seismic isolation bearings including the influence of axial load. Earthquake Eng Struct Dynam 2009;38(2):157–80. http://dx.doi.org/10.1002/eqe.847.
[5] Ryan KL, Kelly JM, Chopra AK. Nonlinear model for lead–rubber bearings including axial-load effects. J Eng Mech 2005;131(12):1270–8. http://dx.doi.org/10.1061/(ASCE)0733-9399(2005)131:12(1270).
[6] Gent AN. Cavitation in rubber: a cautionary tale. Rubber Chem Technol 1990;63(3):49–53. http://dx.doi.org/10.5254/1.3538266.
[7] Takayama M. Ultimate capacity of natural rubber bearings used in seismic isolation system. J Tech Archit Build Sci Inst Jpn 1995;110:160–5.
[8] Buckle I, Nagarajaiah S, Ferrell K. Stability of elastomeric isolation bearings: experimental study. J Struct Eng 2002;128(1):3–11. http://dx.doi.org/10.1061/(ASCE)0733-9445(2002)128:1(3).
[9] Nagarajaiah S, Ferrell K. Stability of elastomeric seismic isolation bearings. J Struct Eng 1999;125(9):946–54. http://dx.doi.org/10.1061/(ASCE)0733-9445(1999)125:9(946).
[10] Koh CG, Kelly JM. A simple mechanical model for elastomeric bearings used in base isolation. Int J Mech Sci 1988;30(12):933–43. http://dx.doi.org/10.1016/0020-7403(88)90075-6.
[11] Chang CH. Modeling of laminated rubber bearings using an analytical stiffness matrix. Int J Solids Struct 2002;39(24):6055–78. http://dx.doi.org/10.1016/S0020-7683(02)00471-7.
[12] Kelly JM. Tension buckling in multilayer elastomeric bearings. J Eng Mech 2003;129(12):1363–8. http://dx.doi.org/10.1061/(ASCE)0733-9399(2003)129:12(1363).
[13] Liu WG, He WF, Feng DM, Yang QR. Vertical stiffness and deformation analysis models of rubber isolators in compression and compression-shear states. J Eng Mech 2009;135(9):945–52. http://dx.doi.org/10.1061/(ASCE)EM.1943-7889.0000010.
[14] Yang QR, Liu WG, He WF, Feng DM. Tensile stiffness and deformation model of rubber isolators in tension and tension-shear states. J Eng Mech 2010;136(4):429–37. http://dx.doi.org/10.1061/(ASCE)EM.1943-7889.0000007.
[15] He WF, Liu WG, Yang QR, Feng DM. Nonlinear rotation and shear stiffness theory and experiment research on rubber isolators. J Eng Mech 2012;138(5):441–9. http://dx.doi.org/10.1061/(ASCE)EM.1943-7889.0000350.
[16] Crisfield MA. A consistent co-rotational formulation for non-linear, three-dimensional, beam-elements. Comput Methods Appl Mech Eng 1990;81(2):131–50. http://dx.doi.org/10.1016/0045-7825(90)90106-V.
[17] Faroughi S. Dynamic nonlinear co-rotational formulation for two-dimensional continua. Latin Am J Solids Struct ABCM J 2014;12(3):477–91.
[18] Chen SC, Tian XK, Yan WM, Kim KS. Modeling and analysis of laminated rubber bearings under axial tensile loading. Mater Struct 2014;47(6):987–97. http://dx.doi.org/10.1617/s11527-013-0108-3.
[19] Kelly JM, Konstantinidis D. Mechanics of rubber bearings for seismic and vibration isolation. John Wiley & Sons; 2011 [chapter 2, 19–32; chapter 3, 45–51; chapter 5, 83–108].
[20] De la Llera JC, Lüders C, Leigh P, Sady H. Analysis, testing, and implementation of seismic isolation of buildings in Chile. Earthquake Eng Struct Dynam 2004;33(5):543–74.
[21] COMSOL Multiphysics 5.0. Protected by US patents 7,519,518; 7,596,474; 7,623,991; 8,219,373; 8,457,932; and 8,626,475. Patents pending © 1998–2014 COMSOL. All rights reserved.
[22] Gent AN, Lindley PB. Internal rupture of bonded rubber cylinders in tension. Proc R Soc Lond A 1959;249(1257):195–205. http://dx.doi.org/10.1098/rspa.1959.0016.
[23] Ismail M, Ikhouane F, Rodellar J. The hysteresis Bouc-Wen model, a survey. Arch Comput Methods Eng 2009;16(2):161–88. http://dx.doi.org/10.1007/s11831-009-9031-8.